Biochemistry and Biophysics Reports 43 (2025) 102128

Contents lists available at ScienceDirect

Biochemistry and Biophysics Reports

journal homepage: www.elsevier.com/locate/bbrep

DODAB-ODN lipoplex structure is highly dependent on ODN concentration: A multitechnique experimental study

Cristofher Victor Vivas [a,1], Antonio R. da Cunha [b], M. Teresa Lamy [a], Evandro L. Duarte [a], Gabriel S. Vignoli Muniz [c,*]

[a] Instituto de Física, Universidade de São Paulo, R. do Matão, 1371, 05508-090, SP, Brazil
[b] Universidade Federal do Maranhão, Campus Balsas, 6500-000, Maranhão, Brazil
[c] Instituto de Química, Universidade de Brasília, (DF), 70919-970, Brasília, Brazil

A B S T R A C T

This study explores the structural properties of lipid vesicles composed of dioctadecyldimethylammonium bromide (DODAB) and varying concentrations of the oligonucleotide 5′-AAAAAAAAAA-3’ (ODN). The vesicles, in both gel and fluid phases, were characterized using dynamic light scattering (DLS), Zeta potential, small-angle X-ray scattering (SAXS), differential scanning calorimetry (DSC), and fluorescence with the fluorescent probe Laurdan embedded into DODAB vesicles. The DODAB-ODN interaction induces concentration-dependent structural changes on the lipoplex. At relatively low ODN concentrations ([ODN]/[DODAB] < 0.050), the dispersion remains stable, with positively charged vesicles, though with an increase in vesicle size and sample turbidity, and SAXS indicates coalescence of vesicles with multilamellar structure formation. DSC revealed the coexistence of ODN-free and ODN-rich regions, with the latter showing increased thermal stability. Laurdan fluorescence indicates that the probe does not significantly partition into the lipoplex ODN-rich regions. At intermediate concentrations ($0.050 <$ [ODN]/[DODAB] < 0.075), colloidal stability is lost, and pure DODAB domains are no longer detected. At relatively high ODN concentrations ($0.075 \leq$ [ODN]/[DODAB] ≤ 0.200), the dispersion is stable, showing a negative vesicle surface potential, and the presence of small multilamellar vesicles. Laurdan lifetimes are significantly increased, suggesting that ODN induces lipid packing or dehydration at the surface of the vesicles in both the gel and fluid phases. These findings enhance our understanding of the structure of lipid-ODN aggregates, paving the way for their application in gene therapy.

1. Introduction

Gene therapy involves the delivery of genetic material to target cells, offering a modern strategy to correct genetic defects, restore normal cellular function, or enhance the immune system [1]. Due to the highly negatively charged nature of genes, they cannot readily cross the plasma membrane, necessitating the use of carriers. While viral vectors are the most commonly used carriers for genetic material, concerns about their toxicity in humans have prompted the scientific community to search for non-viral alternatives [2,3]. Different molecules have been proposed for gene therapy, including peptides, proteins, inorganic and organic nanoparticles, and lipids. Among these, lipid vesicles have emerged as promising candidates and have been widely used for the delivery of genetic material [2,4,5].

Particularly, lipid systems composed of the cationic lipid dioctadecyldimethylammonium bromide (DODAB) have the ability to form lipoplexes by binding nucleic acids and have been successfully used to deliver genetic material to living cells [6–8].

Furthermore, DODAB (Fig. 1) was shown to induce a strong immune response in mammals [9,10], to bind to drugs [11,12] and antigens [13], and act against intracellular parasites [14]. As it interacts with molecules that have potential therapeutic applications [15–17], DODAB is a promising candidate for developing new immunotherapeutic strategies [7,15,18,19].

It has been shown that the physicochemical properties of lipoplexes, such as size, charge density, and colloidal stability, have significant consequences for the efficiency of gene delivery to living cells [20]. Therefore, understanding the physicochemical properties of these systems is essential for engineering new carriers and optimizing existing carrier systems [20].

Concerning the physical properties of DODAB lipoplexes, it has been demonstrated that non-extruded DODAB-1,2-dioleoyl-*sn*-glycero-3-phosphocholine (DOPC) (1:1 M ratio) dispersions undergo significant changes upon binding calf thymus DNA (CT DNA). Dynamic light scattering (DLS) measurements revealed that the initial vesicle size was approximately 500 nm. As the CT DNA concentration increased up to 40

* Corresponding author. Instituto de Química, Universidade de Brasília, (DF), 70919-970, Brasília, Brazil.
E-mail address: gabriel.vignoli@unb.br (G.S. Vignoli Muniz).
[1] Present Address: Universidad Tecnológica del Perú, Lima, Perú.

https://doi.org/10.1016/j.bbrep.2025.102128
Received 20 May 2025; Received in revised form 18 June 2025; Accepted 30 June 2025
Available online 19 July 2025

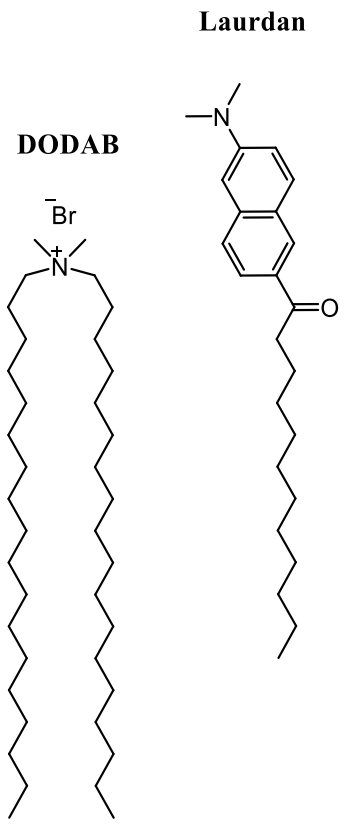

Fig. 1. Chemical structures of DODAB and the fluorescent probe Laurdan.

μg/ml, the vesicle size expanded to around 3500 nm, while the initially positive vesicle surface potential was neutralized. At higher CT DNA concentrations, the surface potential became negative, and the vesicle size decreased, eventually returning to the size of lipid vesicles without CT DNA [21].

Similarly, different amounts of the 5′-TTGACGTTCG-3′ oligonucleotide (CpG) affected DODAB bilayer fragments (DODAB BF) in pure water previously mixed with ovalbumin leading to an increase in vesicle size until the vesicle surface potential was neutralized. At higher CpG concentrations, smaller vesicles were formed, and the surface potential became negative [7].

High concentrations of the 5′-AAAAAAAAAA-3′ oligonucleotide (ODN) (0.4 mM) also altered the structure of non-extruded DODAB dispersions (2 mM) in pure water [22]. Spin labels incorporated at different depths of the DODAB-ODN system revealed that higher ODN concentrations (0.4 mM) rigidified gel-phase DODAB (2 mM) dispersions, both near the DODAB surface and in the inner core of the lipid bilayer. In the fluid phase, a decrease in bilayer order near the surface was observed, along with lipid packing in the inner core of the bilayer [22]. The authors suggested that the interaction with ODN also dehydrates the vesicle surface.

Considering a possible pharmacological use, in the present work, inspired by the findings of Rozenfeld et al. [22], we characterize a more controlled system: extruded DODAB dispersions (100 nm) in buffer solution (10 mM HEPES, pH 7.4) with different concentrations of the 5′-AAAAAAAAAA-3′ ODN. The experiments were conducted with the lipid system in two phases: a more organized and packed (gel) phase and a looser (fluid) phase, both in the absence and presence of ODN. To achieve this, we employed various techniques, including dynamic light scattering (DLS) and Zeta-potential measurements to monitor the size and surface potential of the vesicles. Small-angle X-ray scattering (SAXS) was used to examine the multilamellar structures of the DODAB-ODN complex, while differential scanning calorimetry (DSC) was applied to monitor changes in the thermotropic behavior of the DODAB dispersion upon ODN binding. Lastly, the structure and dynamics of the vesicle surface were investigated using steady-state and time-resolved fluorescence spectroscopy, with the fluorescent probe 2-dimethylamino-(6--lauroyl)-naphthalene (Laurdan; Fig. 1) incorporated into gel and fluid DODAB vesicles, as Laurdan was shown to monitor the surface of DODAB vesicles [23]. The results obtained in this work may have pharmacological relevance, contributing to a better understanding of the interactions between lipid vehicles and genetic material, hence helping the production of new carriers.

2. Material & methods

2.1. Chemicals and reagents

The cationic lipid, dioctadecyldimethylammonium bromide (DODAB – Fig. 1) was purchased from Avanti Polar Lipids Inc. (Birmingham, AL, USA). The fluorescent probe, 2–dimethylamino-(6–lauroyl)-naphthalene (Laurdan) was acquired from Molecular Probes Inc. (Eugene, OR, USA). The ten-base single-stranded oligonucleotide, 3′-AAA AAA AAA A-5’ (ODN) was purchased from Integrated DNA Technologies IDT (Coralville, IA, USA). HEPES buffer (4-(2-hydroxyethyl)-1-piperazineethanesulfonic acid), chloroform and sodium hydroxide were purchased from Merck (St. Louis, MO). Ultrapure water, with resistivity above 18 MΩ cm, was used throughout.

2.2. DODAB laurdan unilamellar vesicles preparation

The preparation of DODAB unilamellar vesicles consists of solubilizing a desired amount of lipid powder in chloroform so as to obtain a clear solution after stirring with the addition of 1 mol % of the fluorescent probe Laurdan, relative to number of DODAB moles. To perform the fluorescence measurements, it was necessary to add the Laurdan fluorescent probe. Thus, all the samples in this work contain Laurdan (1 mol%). For the sake of simplicity, we will refer to the samples as DODAB samples although they all contain Laurdan.

The chloroform lipid solution was dried under a stream of ultra-pure nitrogen gas till a thin film of lipids was formed at the bottom of the glass tube. Then, the lipid film was kept under low pressure conditions for a minimum of 3 h to eliminate any trace of chloroform. DODAB dispersions were obtained by the addition of buffer (10 mM HEPES, pH 7.4) to the lipid film. The dispersions were maintained at temperatures above DODAB gel-fluid phase transition ($\geq$60 °C) for 30 min, and every 10 min they were vigorously stirred. Finally, lipid dispersions were extruded through polycarbonate filters (mini-extruder by Avanti Polar Lipids, 19 mm membranes with 100 nm pores, 31 times) above the lipid gel−fluid transition temperature ($\geq$60 °C), for the formation of Large Unilamellar Vesicles (LUVs).

2.3. DODAB-ODN vesicles preparation

A stock ODN solution was prepared solubilizing the oligonucleotide in buffer. The ODN concentration was determined by using a molar extinction coefficient at 260 nm equals to 123,400 M^{-1} cm^{-1}, provided by the Integrated DNA Technologies IDT (Coralville, IA, USA). Aliquots of the stock solution were added to DODAB dispersion to achieve the desired concentration. The samples were incubated at room temperature for at least 30 min just prior to the experiments. In this work, we investigated DODAB dispersions in the absence and in the presence of defined concentrations of ODN.

2.4. Hydrodynamic diameter and zeta-potential determination

Measurements were performed using a ZetaSizer, model Nano – ZS^{90} (Malvern Instruments Ltd., Worcestershire, UK), equipped with a 530 nm laser and a temperature controller.

Particle hydrodynamic diameter (D_z) of 1 mM DODAB dispersions, in the absence and presence of ODN, was determined by dynamic light scattering (DLS). Samples were placed in quartz cuvette (1.0 × 1.0 cm, 1 mL), the temperature was kept at 20 °C and the light scattering angle at 90°.

Zeta-potential, ζ, was determined from electrophoretic mobility, μ, measurements, using the Helmholtz - Smoluchowski' mobility equation, ($\zeta = \mu\eta/\varepsilon$), where η and ε are the viscosity and dielectric constant of the medium, respectively [24]. Around 0.6 mL of samples were placed in an appropriate Malvern capillary cell (DTS-1060) with electrodes. The temperature was kept at 20 °C and the light scattering angle at 17 °. It is important to point out that Laurdan, present in the samples, does not have any absorption band around 530 nm.

2.5. Differential scanning calorimetry (DSC)

DSC thermograms were obtained with a Microcal VP-DSC Microcalorimeter (Microcal Inc., Northampton, MA, USA) equipped with 0.5 mL twin total-fill cells. Endothermic and exothermic scans were performed for 1 mM DODAB dispersions in the absence and presence of ODN, at a scan rate of 20 °C/h, from 20 to 60 °C. Scans were performed at least in duplicate. Baseline corrections and peak analysis were done using the Microcal Origin software. The thermodynamic parameters, enthalpy of the transition, ΔH, main gel-fluid phase transition temperature, T_m, and width at half maximum, $\Delta T_{1/2}$, were obtained.

2.6. Small angle X-ray scattering (SAXS)

Small angle X-ray scattering (SAXS) measurements were performed using a Xenocs equipment (Grenoble, France), model Xeuss™, located at the Laboratory of Complex Fluid Group at the Institute of Physics of the University of São Paulo. The X-ray wavelength used corresponds to the Cu Kα line (λ = 1.54 Å). The effective interval of the scattering vector ($= \frac{4\pi}{\lambda}\sin\theta$, where 2θ is the scattering angle) was from 0.5 up to 4.0 nm^{-1}. Samples were placed in a capillary sample holder with 1.5 mm diameter. Measurements were carried out at 30 °C (the lipid gel phase) and 60 °C (fluid phase). Data were corrected by the background scattering obtained by the buffer sample transmission and normalized for the acquisition time.

2.7. Ultraviolet–visible (UV–vis) absorption measurements

UV–vis absorption spectra were acquired using a Varian Cary 50 spectrophotometer (Santa Clara, CA, USA). Measurements were conducted in quartz cuvettes (0.2 × 1.0 cm, 400 μL) with a 0.2 cm optical path length. Temperature was controlled throughout the experiments using a Cary Peltier temperature controller.

The samples consisted of 250 μM DODAB extruded vesicle dispersions labeled with 2.5 μM Laurdan, with or without a defined concentration of oligonucleotide (ODN). Prior to data collection, samples were equilibrated at 30 °C, corresponding to the gel phase of DODAB–ODN systems. To ensure thermal equilibration, the cuvettes were held inside the spectrophotometer for 20 min before initiating measurements. The experimental sequence—UV–vis absorption, steady-state fluorescence, and time-resolved fluorescence—was performed at 30 °C, following the approach described in Ref. [25]. Subsequently, the temperature was raised to 60 °C to investigate the systems under fluid-phase conditions.

2.8. Steady-state fluorescence measurements

Steady-state fluorescence spectra were recorded using a Varian Eclipse spectrofluorometer (Santa Clara, CA, USA), with temperature control provided by a Cary Peltier system. Excitation was performed at 340 nm using a 0.2 cm path length in a quartz cuvette (0.2 × 1.0 cm, 400 μL). Both excitation and emission slits were set to 5 nm.

To correct for inner filter effects, all emission spectra were processed using Equation (1):

$$F_{corr}(\lambda) = F_{obs}(\lambda)10^{(A_{exc}\,l + A_{ems}(\lambda)\,l)} \quad \text{Eq. 1}$$

In this equation, $F_{corr}(\lambda)$, $F_{obs}(\lambda)$ are the corrected and raw fluorescence intensities, respectively. A_{exc}, $A_{ems}(\lambda)$ correspond to the absorbance per unit optical path at the excitation and emission wavelengths, respectively. The excitation and emission path lengths were 0.1 cm and 0.5 cm, respectively, calculated from the center of the cuvette. This correction model does not account for the spatial dimensions of the excitation volume, assuming instead that all emitting molecules are located at the cuvette center. Prior studies have demonstrated that Equation (1) is appropriate for the absorbance levels used in this work [26].

2.9. Time-resolved fluorescence measurements

Time-resolved fluorescence data were acquired using the time-correlated single photon counting (TCSPC) method. The excitation source was a titanium-sapphire laser (Tsunami 3950, Spectra Physics, Newport Corporation, Irvine, CA, USA), pumped by a Millenia Pro J80 solid-state laser (Spectra Physics). The pulse picker (model 3980–25, Spectra Physics) operated at 8 MHz. The Tsunami laser emitted at 852 nm, and a BBO crystal (GWN-23PL, Spectra Physics) was used to generate the third harmonic, resulting in excitation at 284 nm.

Although 284 nm does not correspond to the excitation wavelength employed in steady-state fluorescence measurements (340 nm), it is nonetheless encompassed within an absorption band of Laurdan. Notably, Laurdan's fluorescence relaxation dynamics are well-documented to be independent of the excitation wavelength [23], and the use of 284 nm significantly enhanced the signal-to-noise ratio, as previously implemented in Ref. [25]. Fluorescence emission at 480 nm was collected at a 90° angle with respect to the excitation beam and selected through a monochromator. Decay curves were fitted using the FAST software provided by Edinburgh Photonics, employing a multi-exponential decay model as given in Equation (2):

$$F(\lambda, t) = \sum_{i=1}^{N} \alpha_i e^{-t/\tau_i} \quad \text{Eq. 2}$$

Here, $F(\lambda, t)$ represents the fluorescence intensity at a given wavelength and time, α_i is the pre-exponential factor, and τ_i is the lifetime of the i-th component. The quality of the fits was assessed using the reduced chi-square statistic, with acceptable values ranging from 0.80 to 1.33. All experiments were performed at least twice. Uncertainties correspond to standard deviations and are presented as error bars when larger than the data point symbols.

3. Results and discussions

3.1. Colloidal stability

The presence of ODN changes the turbidity of DODAB dispersions, in a concentration dependent manner. That effect is evident and can be observed with naked eyes (Fig. SM1). At [ODN]/[DODAB] relative molar concentrations up to 0.050, there is an increase in the turbidity of colloidal dispersions, suggesting a coalescence of DODAB vesicles. At [ODN]/[DODAB] relative concentrations from around 0.050 to 0.075 the colloidal stability is lost with a clear colloidal precipitation.

Interestingly, by further increasing the amount of ODN, with [ODN]/[DODAB] relative concentrations ranging from 0.100 to 0.200, the lipid dispersion becomes clearer, showing turbidity levels similar to those obtained for samples at low oligonucleotide concentrations, thus restoring colloidal stability (Fig. SM1). Consequently, there are two regimes of ODN concentration where colloidal stability occurs: a low concentration region, where [ODN]/[DODAB] is below 0.050, and a high concentration regime, above 0.075.

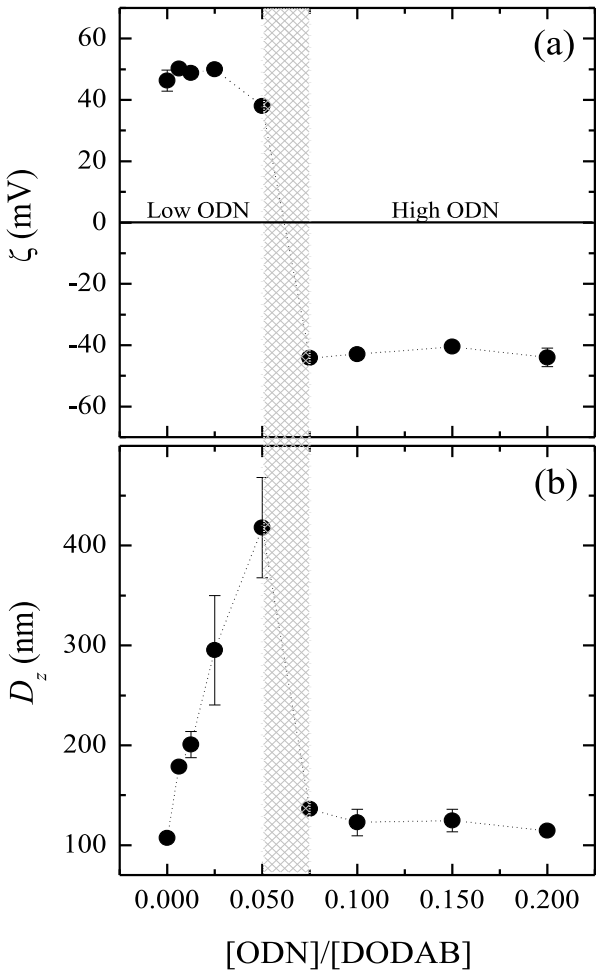

Fig. 2. Zeta-potential ζ (a) and hydrodynamic diameter D_z (b) of 1 mM DODAB liposomes in the absence and in the presence of different concentrations of ODN. The temperature was kept at 20 °C, corresponding to the gel phase of DODAB. The hatched area represents the colloidal unstable region dividing the low and high ODN concentration regimes. Dotted lines are only guides for the eyes.

An important parameter for analyzing the lipid-oligonucleotide interaction is the Zeta potential (ζ), which is widely used to determine the stability of particles in solution, as it is a measurement of the effective particle surface potential when in movement, hence reflects the degree of repulsion between particles. This parameter can be either positive or negative, depending on the electric charges at the particle surface. Colloidal stability occurs when the magnitude of the surface electric potential is sufficiently high, promoting a strong degree of repulsion between particles, regardless of the nature of the charge. On the other hand, dispersions with a Zeta potential close to neutrality (~0 mV) exhibit a low degree of repulsion between particles, favoring coalescence and colloidal precipitation [27]. Complementary to the Zeta potential data, the hydrodynamic diameter (*Dz*) and the polydispersity index (PI), obtained through dynamic light scattering (DLS), provide insight into the size of the particles and the polydispersity of the colloidal dispersion. The results in Fig. 2 clearly show the effect of increasing the ODN concentration in DODAB dispersions, using surface charge, size, and size distribution parameters at 20 °C (DODAB gel phase). Measurements at 60 °C, DODAB fluid phase, were found difficult to be reproduced, possibly due to bubbles formation at this temperature, so only data at 20 °C are presented.

Zeta potential (ζ) results obtained from dispersions of 1 mM DODAB in the absence and presence of different concentrations of ODN at 20 °C are shown in Fig. 2a. Data are divided into two ODN concentration regimes where the dispersions are quite stable, separated by a hatched region corresponding to the region where there is no colloidal stability. In the absence of ODN, DODAB dispersions present ζ values of +50 ± 2 mV. As the [ODN]/[DODAB] relative molar concentration increases within the low ODN concentration regime, ζ decreases to around +38 ± 1 mV, strongly indicating that the highly anionic ODN molecules are being incorporated into DODAB vesicles. In contrast, in the high ODN concentration regime, the vesicle surface charge becomes negative, driven by the excess of ODN in the DODAB vesicles, with ζ values around −44 ± 2 mV.

Fig. 2b shows the hydrodynamic diameter (*Dz*) results from the same samples studied for Zeta potential, as a function of the [ODN]/[DODAB] relative concentration. It is interesting to observe that even at very low ODN concentrations, up to [ODN]/[DODAB] = 0.025, *Dz* increases significantly while the zeta potential does not change much. That parallels an increase in the data standard deviations, as shown in Fig. 2. That can be understood considering an increase in polydispersion, and how small amounts of larger particles strongly affects *Dz* measurements [28], since dynamic light scattering is highly sensitive to the presence of even a small fraction of larger aggregates due to the intensity of scattered light scaling with the sixth power of the particle radius.

As the ODN concentration increases, *Dz* also increases, reaching a maximum of ~420 ± 50 nm with the addition of 0.050 mM ODN. Considering the DLS data (Fig. 2), the increase in turbidity can be interpreted as vesicle coalescence or aggregation due to the shielding (or neutralization) of positive charges on the external surface of the DODAB vesicles. In the high ODN concentrations regime, *Dz* decreases to a value similar to that of DODAB dispersion in the absence of oligonucleotide, *Dz* ~115 ± 5 nm, in the same region where the charge polarity inversion occurs from the Zeta potential values (Fig. 2a). This result demonstrates that in the high ODN concentration regime, there is an arrangement with excess negative charges at the DODAB vesicle surface, hence a repulsive potential between vesicles. Rozenfeld et al. [29] investigated the interaction of ODN with DODAB bilayer fragments in pure water and reported a behavior similar to ours: at a [ODN]/[DODAB] ratio of 0.050, *Dz* values increased, indicating the neutralization of DODAB-ODN particles. Higher ODN concentrations induced a polarity inversion, resulting in *Dz* values comparable to those of pure DODAB dispersions. A similar behavior was observed (as seen for low and high ODN contents) in lipid dispersions containing DODAB and varying amounts of CT DNA [21].

It is worth mentioning that all results presented here were obtained with an incubation time of ~30 min after the addition of ODN into DODAB dispersions. To test a longer period of stability for these samples, having in mind their possible use in pharmacology, new ζ and DLS measurements were performed after 7 days of incubation at 20 °C. Interestingly, the dispersions, with the exception of the 0.075 mM ODN sample, showed high stability, as demonstrated by the surface potential and vesicle size (*Dz*) (Fig. SM2).

3.2. ODN induces coalescence in DODAB extruded vesicles

DLS measurements show a substantial increase in vesicle size (Fig. 2b), as previously reported for the interaction between cationic lipid systems and genetic material [21,22,29], which could be due to vesicle aggregation or coalescence. Consequently, we performed Small-angle X-ray scattering (SAXS) experiments to investigate the lipid-ODN system. SAXS is a powerful tool for studying liposome structure. For instance, multilamellar vesicles can be identified from the SAXS curve by the appearance of Bragg peaks (or interference peaks) [30,31]. Furthermore, the repetition distance between the multilamellae, that is, the thickness of the lipid bilayer plus the water layer, *d*, can be calculated using the expression $d = \frac{2\pi}{q_{peak}}$, where q_{peak} is the scattering vector (see section 2.6) [32]

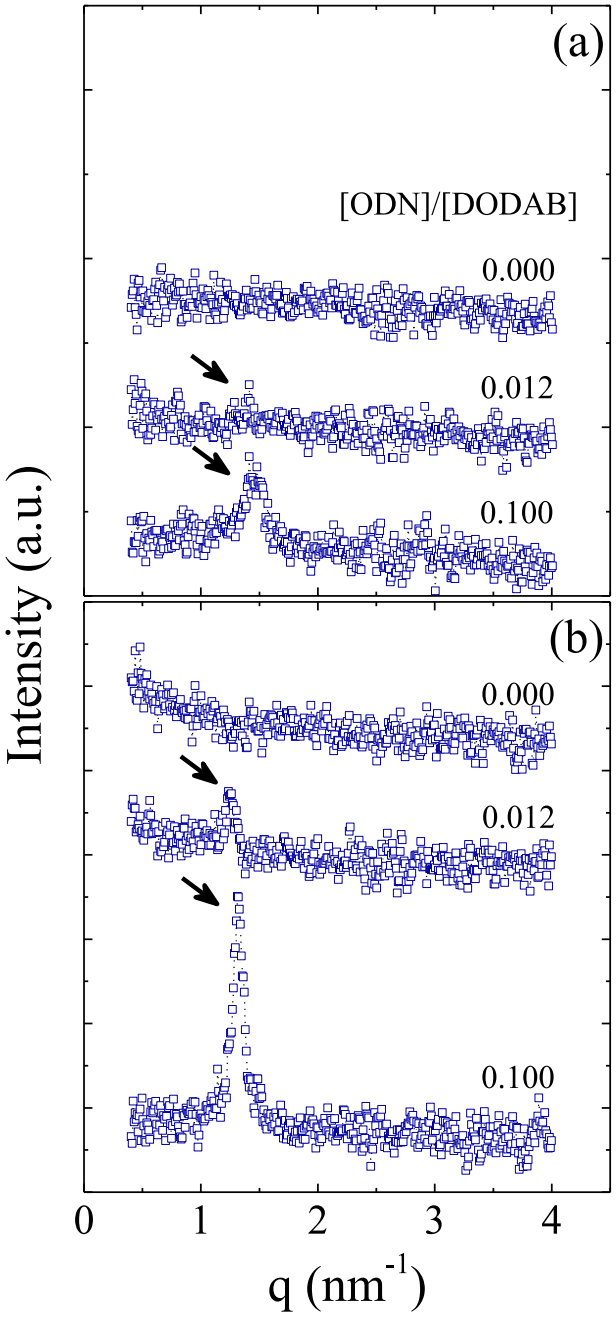

Fig. 3. SAXS diffractograms of extruded DODAB dispersions in the absence and in the presence of low (0.012 mM) and high (0.100 mM) ODN concentration at: (a) 30 °C and (b) 60 °C. Interference peaks are indicated by the arrows. Graphs have the same intensity scale, and the curves are shifted for better visualization.

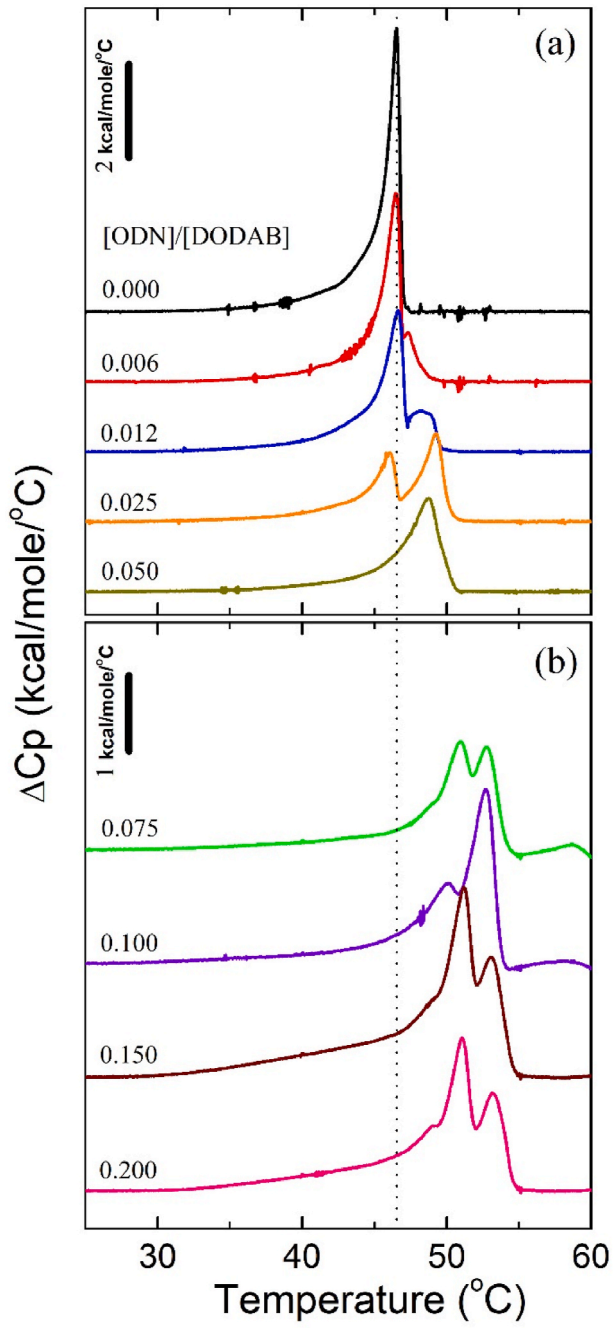

Fig. 4. Typical excess heat capacity (ΔCp) profiles of 1 mM DODAB in the absence (black lines) and in the presence of ODN divided into two regimes: (a) low ODN concentrations, from 0.006 up to 0.050 mM and (b) high ODN concentrations, from 0.075 up to 0.200 mM, as indicated in the figures. The dashed line indicates the position of the gel-to-fluid transition of pure DODAB vesicles.

In this work, we present SAXS diffractograms obtained for the extruded lipid dispersions of DODAB in the absence and presence of ODN. We selected samples at [ODN]/[DODAB] concentrations of 0.012, representing the low ODN concentration regime, and samples at [ODN]/[DODAB] = 0.100, representing the high ODN concentration regime (according to Fig. 2), to perform SAXS experiments. The measurements were conducted at temperatures of 30 °C (Fig. 3a) and 60 °C (Fig. 3b), corresponding to the DODAB gel and fluid phases, respectively.

For both temperatures, in the absence of ODN, the scattering curves do not show diffraction peaks, indicating that DODAB LUV dispersions are composed of unilamellar vesicles with sufficient charge to ensure the presence of vesicles with just one lamella and colloidal stability. Even non extruded DODAB dispersions were shown to be composed of stable unilamellar vesicles, due to the high charge at the vesicle surface [22, 33]. The addition of 0.012 mM ODN reveals a low-intensity diffraction peak at 30 °C (indicated by the arrow in Fig. 3a) at $q_{peak} = 1.4$ nm^{-1}, corresponding to a repetition distance d = 4.5 nm. As the temperature increases to 60 °C (Fig. 3b) the interfering signal becomes more evident, with the maximum diffraction peak at $q_{peak} = 1.3$ nm^{-1}, corresponding to a repetition distance d = 4.8 nm. This increase in bilayer width is typical during the transition from the gel to the fluid phase in most lipids. It results from enhanced thermal motion of the lipid molecules, leading to greater disorder in the acyl chains and a reduction in lateral packing density, which in turn causes a slight swelling of the bilayer [33,

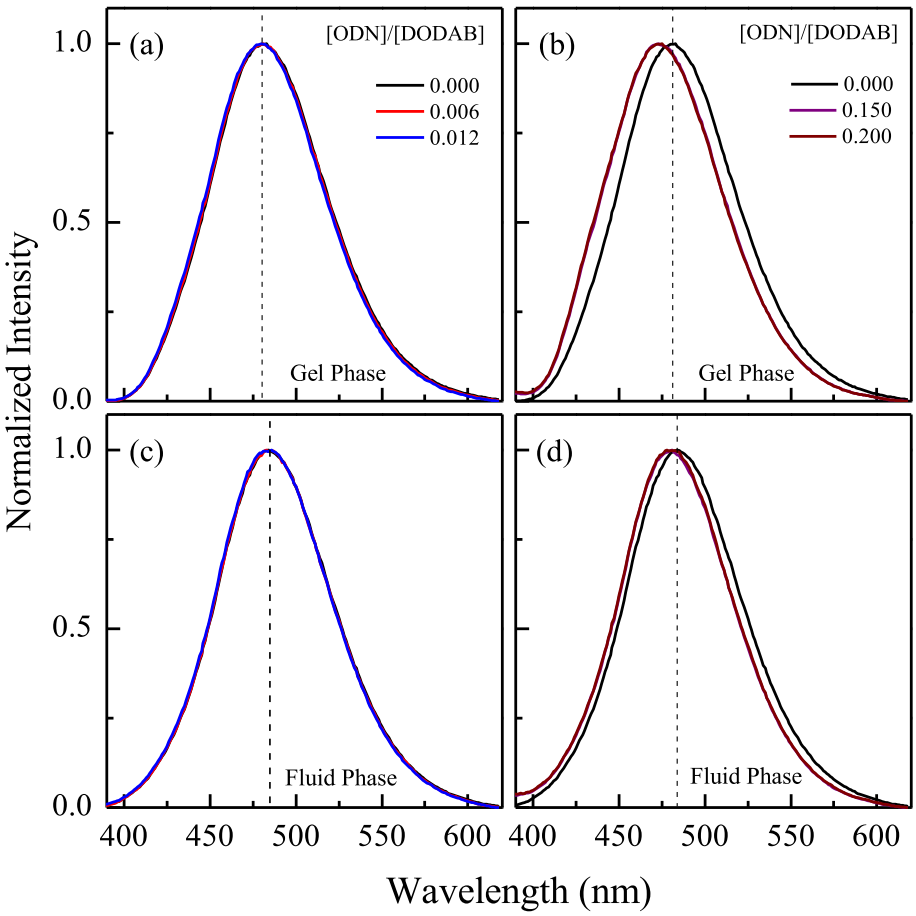

Fig. 5. Typical fluorescence spectra of 2.5 μM Laurdan incorporated into 250 μM DODAB vesicles in the absence and in the presence of: (a and c) low relative [ODN]/[DODAB] concentrations (0.006 and 0.012), and (b and d) high [ODN]/[DODAB] concentrations (0.150 and 0.200), in the gel phase at 30 °C (a and b) and fluid phase at 60 °C (c and d). Dotted lines indicate the maximum emission wavelength of pure DODAB. Excitation at 340 nm.

34]. The formation of multilamellar structures arises from the association between the cationic DODAB vesicles and the oligonucleotide (ODN), and not from the DODAB dispersion alone.

In the regime of high ODN concentrations, [ODN] = 0.100 mM, the Bragg peak is clearly present at both temperatures (Fig. 3a and b), with the same repetition observed for the dispersion at low concentration of ODN, with d = 4.5 nm at 30 °C and 4.8 nm at 60 °C. The repetition distances observed here are similar to those reported for non-extruded DODAB water dispersions with high ODN concentrations ([ODN]/[DODAB] = 0.2) [22].

Interestingly, the intensity of the Bragg peak increases with high ODN concentrations (Fig. 3). On the other hand, DLS data show that the average size of the gel-phase liposomes remains almost unchanged for this ODN concentration regime (Fig. 2). This suggests that the number of lamellae per DODAB-ODN gel liposome is similar at both high and low ODN concentrations. Therefore, the increase in Bragg peak intensity can be interpreted as an increase in the relative number of multilamellar gel liposomes, rather than an increase in the number of lamellae per liposome as the ODN concentration rises.

3.3. Thermal effect induced by ODN in DODAB vesicles

Differential scanning calorimetry (DSC) is a valuable technique to investigate lipid systems, as it reveals thermal events associated with phase transitions. The thermotropic behavior of lipids can be influenced by exogenous molecules that disrupt lipid packing or the order of acyl chains, given that the gel-fluid lipid transition depends on lipid-lipid interactions [35]. Consequently, DSC is well-suited for studying the interaction between lipid systems and membrane-active molecules. Fig. 4 presents the DSC thermograms of DODAB dispersions with and without specific ODN concentrations.

DODAB dispersions display a peculiar thermal transition, with a significant hysteresis under endothermic and exothermic processes [36–38]. Accordingly, we observed T_m at (46.5 ± 0.1) °C and (41.0 ± 0.1) °C, for endothermic and exothermic processes (Table SM1 e Fig. SM3), respectively. Furthermore, DODAB dispersions without ODN display a ΔH equals to (9 ± 2) kcal/mol and (-10 ± 2) kcal/mol (endothermic and exothermic, respectively, Table SM1**)**. All samples used in this study contain 1 mol% Laurdan, and the thermodynamic parameters (T_m and ΔH) are, within experimental error, consistent with those reported for pure DODAB [23,37]. In addition, the DSC thermograms of pure DODAB and DODAB containing 1 mol% Laurdan are very similar (Fig. SM4), reinforcing that this Laurdan concentration does not significantly affect the thermotropic behavior of DODAB membranes.

Low [ODN]/[DODAB] relative concentrations, specifically 0.006, 0.012, and 0.025, induce a new thermal event at a higher temperature (~49 °C) that coexists with the gel-fluid transition peak of pure DODAB (~46 °C), which decreases in intensity as the ODN concentration increases. This coexistence of thermal events has been associated with the formation of molecule-bound and molecule-free regions in membrane [25,39,40]. This effect has also been correlated with a strong electrostatic interaction between an exogenous molecule and an ionic bilayer surface.

At a relative [ODN]/[DODAB] concentration of 0.050, only one thermal peak is observed at 49 ± 1 °C. This is in accord with the decrease of the vesicle surface potential and the beginning of the

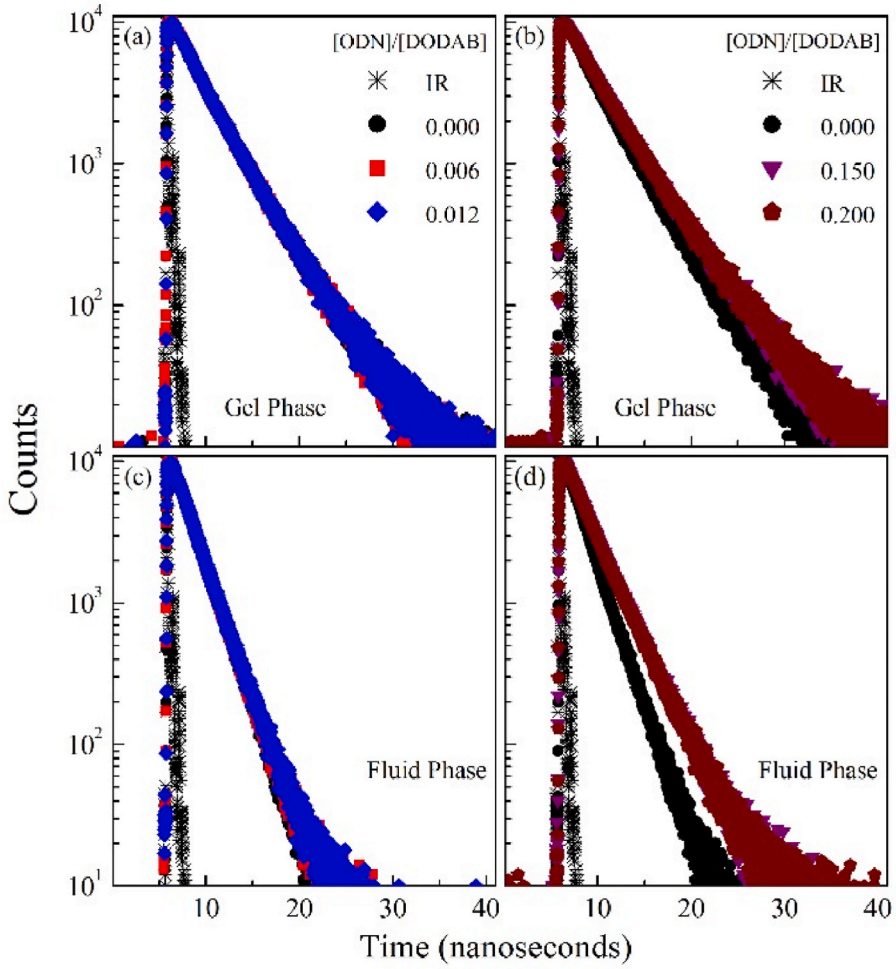

Fig. 6. Laurdan fluorescence decay incorporated into 250 μM DODAB vesicles in the absence (black circles) and in the presence of: (a and c) low relative [ODN]/[DODAB] concentrations (0.006 red squares and 0.012 blue diamonds), and (b and d) high [ODN]/[DODAB] concentration (0.150 down purple triangles and 0.200 wine pentagons), in the gel phase, at 30 °C (a and b), and fluid phase at 60 °C (c and d). IR is the instrument response. Excitation at 284 nm and emission at 480 nm.

colloidal unstable region (Fig. 2a), where vesicle surface charge is neutralized, hence no thermal transition associated with pure DODAB gel-fluid transition is expected. Moreover, the interaction with ODN yields thermograms wider than that observed for pure DODAB dispersion indicating that ODN molecules are disrupting the interactions among DODAB molecules.

In the high ODN region, with negatively charged vesicles, as indicated by the Zeta-potential (see Fig. 2a), the gel-fluid transition temperature occurs at a much higher temperature value, around 53°C, indicating that ODN does stabilize the gel phase of the mixed vesicle. It is also a complex thermal event, with at least two main picks, but none of them corresponding to pure DODAB bilayer. Similar thermal profiles were obtained before [22,29] for the interaction of high ODN content with non-extruded DODAB and DODAB bilayer fragments.

3.4. High ODN content leads to packing and/or dehydration at the DODAD-ODN liposome surface

Laurdan is a very useful fluorescent probe to investigate dynamics/structure of amphiphilic aggregates, and changes induced on them by exogenous molecules [25,41–43], as Laurdan acyl tail ensures that this probe stays into the lipid bilayer, not partitioning in the aqueous environment [44,45]. In phospholipid bilayers, it has been proposed that the Laurdan fluorescent moiety resides within the membrane near the polar headgroups of the lipid bilayers, thereby probing that region [42,46].

Laurdan was reported to be very sensitive to changes in membrane polarity and/or packing [45,47]. Accordingly, when Laurdan vicinity becomes more hydrated, Laurdan emission is shifted to higher wavelengths (smaller energies), as the dipolar relaxation increases considerably [44]. Particularly, when incorporated into phospholipid bilayers, Laurdan emission displays a significant red shift (~50 nm) along the gel-fluid transition of phospholipid membranes [48]. Aside from that, it has been shown that Laurdan is sensitive to changes in phospholipid bilayer structure due to temperature variations, and changes induced in a fluid phospholipid bilayer structure by exogeneous molecules [46,49].

Interestingly, Laurdan emission in DODAB vesicles does not present a significant redshift when DODAB membranes go through gel-fluid transition [23]. Hence, it has been proposed that when incorporated into DODAB bilayers, the Laurdan fluorescent moiety is positioned at the surface of the bilayer, probing the polarity, structure and dynamics of the vesicle surface [23]. As it has been suggested that ODN can change the hydration of the DODAB surface [22], we considered it important to investigate the DODAB-ODN vesicle by using Laurdan, a probe located at the DODAB surface.

Fig. 5 shows Laurdan emission within gel (Fig. 5a and b) and fluid (Fig. 5c and d) DODAB vesicles in the absence (black lines) and with different [ODN]/[DODAB] relative molar concentrations, corresponding to low (Fig. 5a and c) and high (Fig. 5b and b) ODN concentration regimes. Laurdan emission in pure DODAB vesicles displays maxima at 482 nm and 484 nm, for gel (30 °C; Fig. 5a and b) and fluid (60 °C;

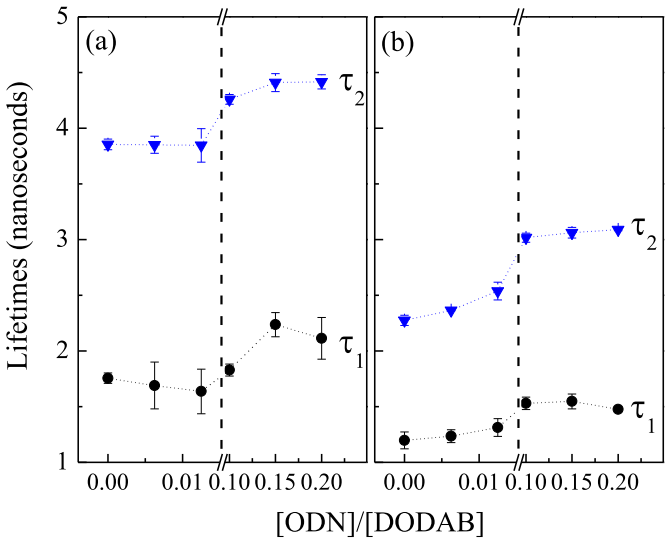

Fig. 7. Fluorescence emission lifetimes of Laurdan incorporated into gel-phase (30 °C) (a) and fluid-phase (60 °C) (b) DODAB liposomes as a function of the relative [ODN]/[DODAB] molar ratio. The dashed line separates the low and high ODN concentration regimes. The dotted lines are provided as guides to the eyes.

Fig. 5c and d) vesicles, respectively, in accordance with previous data [23].

The presence of ODN in the low concentration regime has no significant impact on the profile of Laurdan emission spectra either at the gel (Fig. 5a) or fluid (Fig. 5c) phases. In contrast, at high ODN concentrations (0.150 and 0.200), the Laurdan emission profile exhibited a blue shift of 11 nm and 4 nm, for gel (Fig. 5b) and fluid (Fig. 5d) DODAB vesicles, respectively. These results reinforce the previous hypothesis [22] that at higher concentrations, ODN could cause dehydration at the surface of DODAB vesicles. Those results are particularly interesting as Laurdan was shown to be insensitive to changes in the polarity/structure/dynamics of gel phospholipid bilayers induced by exogenous molecules that penetrate the lipid bilayer such as cholesterol and membrane-disrupting peptides [40] and references therein. Hence, that indicates that both ODN and Laurdan fluorescent moiety are localized at the surface of the DODAB bilayer, at a rather shallow position.

Light scattering can strongly affect fluorescence spectra. Although the fluorescence spectra presented here were corrected (Eq. (1)) using the measured absorbance values (Fig. SM5), we found important to employ a complementary technique. Therefore, time-resolved fluorescence was also applied. This approach, which is minimally impacted by light scattering [50], enables us to determine excited-state lifetimes by measuring the fluorescence decay. In this context, Fig. 6 shows Laurdan decay into DODAB (30 °C) gel (Fig. 6a and b) and (60 °C) fluid (Fig. 6c and d) vesicles, in the absence (black circles) and with different [ODN]/[DODAB] relative molar concentrations, corresponding to low (Fig. 6a and c) and high (Fig. 6b and d) ODN concentration regimes. It has been shown that fluorescence decay curves of Laurdan, whether in organic solvents or within amphiphilic aggregates, can be fitted using a biexponential model, resulting in two distinct fluorescence lifetimes [23,47], and the references therein. Accordingly, all decay curves (Fig. 6) were satisfactorily fitted with two exponential components, meeting the appropriate statistical criteria.

Laurdan in pure DODAB vesicles displays two lifetimes, a short (τ_1) and a longer (τ_2) lifetime. The values found were $\tau_1 = (1.75 \pm 0.06)$ ns and $\tau_2 = (3.82 \pm 0.04)$ ns for gel (30 °C), and τ_1 (1.1 ± 0.1) and $\tau_2 = (2.31 \pm 0.05)$ for fluid (60 °C) vesicles. The values found here are similar to those reported in the literature [23]. As expected, the lifetimes at fluid phase (60 °C) are smaller in comparison with those found at gel phase, 30 °C. This is due to the increase in the rate of the non-radiative decay processes as temperature rises [44]. Fig. 7 shows the evolution of the Laurdan lifetimes as a function of ODN concentration, for gel (30 °C) and fluid (60 °C) DODAB vesicles.

Laurdan decay in the presence of low ODN concentrations at 30 °C (Fig. 6a) and at 60 °C (Fig. 6c) seems to be rather similar to that found for pure DODAB. In contrast to this, high ODN contents evidently change the Laurdan decay profile at 30 °C (Fig. 6b), with the changes becoming more evident in the Laurdan decay spectra at 60 °C (Fig. 6d).

To better understand the effects of ODN on DODAB vesicles, we decomposed all the fluorescence decays using Eq. (2). All the decay curves (Fig. 6) could be well fitted with two exponential decays, satisfying the statistical criterion. Fig. 7 displays the shorter lifetimes, τ_1, (black circles) and the longer lifetimes, τ_2, (blue down triangles).

Similar to the results obtained with the Laurdan emission spectrum (Fig. 5a and c), in the low concentration regime, ODN does not notably affect Laurdan lifetimes in either thermal phase (Fig. 7). Although DLS measurements (Fig. 2) indicate that ODN interacts with DODAB vesicles, and the DSC thermograms strongly suggest the formation of ODN-rich and ODN-free regions on DODAB membranes, it is possible that the fluorescent probe does not partition into ODN-rich domains, thereby detecting only minor changes induced on the membrane.

Again, similar to the results obtained with steady state fluorescence (Fig. 5b and d), high ODN concentrations significantly enhance Laurdan lifetimes in both gel (Fig. 7a) and fluid (Fig. 7b) lipid system phases. Usually, fluorophores in more rigid and non-polar environments display longer lifetimes than those observed for fluorophores in more fluid/hydrated environments. Thus, the increase in lifetimes suggests that ODN is inducing lipid packing in the nanoregion of the probe and/or decreasing polarity, as indicated by the steady state fluorescence measurements (Fig. 5b and d), and as suggested by Rozenfeld et al. [22]. In addition, it is important to point out that in this concentration regime, Zeta-potential data (Fig. 2a) indicate the DODAB vesicles become anionic, strongly suggesting the absence of free-ODN regions on DODAB membranes. Consistently, DSC thermograms show no DODAB-free regions (Fig. 4b), implying that Laurdan is monitoring the densely packed and/or dehydrated DODAB-ODN membrane surface.

Important to point out that the information obtained with Laurdan is complementary to that obtained with spin labels, in the high ODN concentration regime [22], as Laurdan monitors the surface of the DODAB-ODN bilayer, and the used spin labels monitored the bilayer around the 5th carbon atom and at its core. Hence, compiling the data obtained with Laurdan (Figs. 5–7) and spin labels [22], for the bilayer gel phase, ODN induces bilayer packing and/or dehydration at the membrane surface, and packing along the hydrocarbon chain, both at the 5th carbon atom region, and at the bilayer core. Interestingly, in fluid membranes, ODN induces packing and/or dehydration at the surface (Figs. 5–7), but somehow more fluidity/disorder around the 5th carbon atom and more rigidity/order at the bilayer core [22].

4. Conclusions

This work shows that ODN strongly interacts with DODAB cationic vesicles in a concentration-dependent manner and characterizes three distinct behaviors regarding colloidal stability and vesicles structure with different techniques.

At relatively low ODN concentrations ([ODN]/[DODAB] < 0.050), ODN induces an increase in vesicle size and a decrease in vesicle surface potential (Fig. 2). SAXS scattering profiles indicate vesicles coalescence and the formation of multilamellar structures of few lamellae and/or a not well-organized structure, evident due to the presence of a large and not well-defined Bragg peak (Fig. 3b). DSC traces reveal two distinct transition events, indicating the coexistence of ODN-poor and ODN-rich domains in DODAB membranes, the latter being thermally more stable (Fig. 4a). Laurdan emission spectrum and fluorescence decay show similar profiles for gel and fluid DODAB vesicles in the presence and

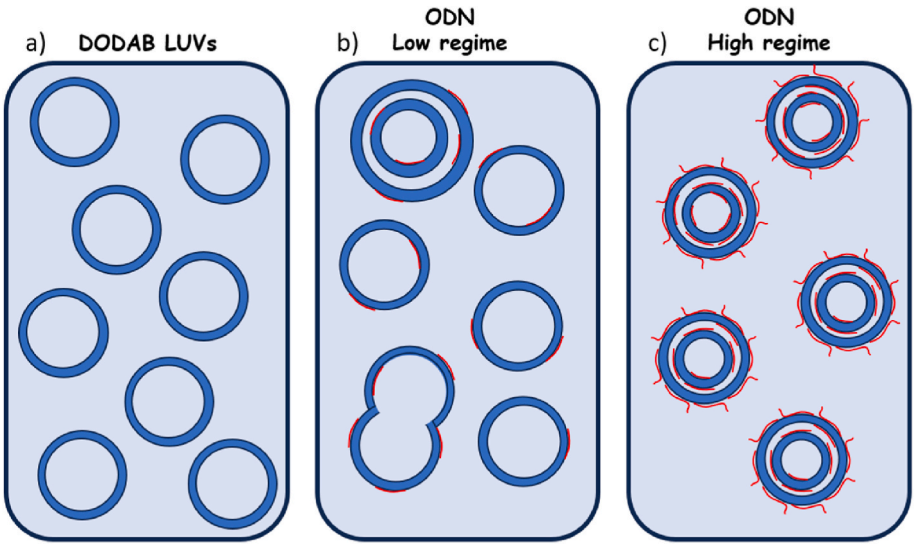

Fig. 8. Schematic model of pure DODAB large unilamellar vesicles (LUVs) (a), DODAB vesicles in the presence of low ODN concentration (b), and DODAB vesicles in the presence of high ODN concentration (c). The blue circles represent the DODAB bilayers, and the red traces represent the anionic ODN molecules.

absence of ODN (Figs. 5–7). Since different techniques, DSC, DLS and SAXS, monitor changes in DODAB structure, probably the fluorescent probe does not partition into the thermally more stable membrane domains.

At relatively intermediate [ODN]/[DODAB] concentrations (0.050–0.075), colloidal stability is lost, and pure DODAB domains are no longer detectable in DSC thermograms (Fig. 4). Hence, spectroscopic measurements over this relative concentration range are unavailable due to significant light scattering.

At relatively higher [ODN]/[DODAB] concentrations, above 0.075, the lipid dispersion is stable, with a negative vesicle surface potential as indicated by Zeta potential measurements (Fig. 2a). DLS measurements show the presence of small vesicles like in pure DODAB dispersion (Fig. 2b), though SAXS measurements indicate multilamellar structures at both DODAB phases (Fig. 3b), hence the presence of vesicles with few lamellae. In this concentration range, DSC traces indicate high thermal stability of the gel phase (high gel-fluid transition temperature, Fig. 4b), and the fluorescent probe Laurdan monitors variations at the membrane surface, indicating a decrease in solvent molecules around the probe and/or a membrane packing caused by ODN at the DODAB vesicle surface (Figs. 5–7).

To summarize and illustrate these findings, we included a schematic model of the lipoplexes in Fig. 8. This model depicts the structural arrangements and colloidal behaviors observed at different ODN concentrations.

Considering the biological interest, we hope that the results presented in this study will contribute to a better understanding of the interaction between ODN and DODAB vesicles, potentially aiding in the development of more effective delivery systems. Overall, this study contributes to a deeper understanding of the structural and colloidal features governing DODAB–ODN assemblies, an essential step toward the rational design of more effective gene delivery systems.

Declaration of competing interest

The authors declare that they have no known competing financial interests or personal relationships that could have appeared to influence the work reported in this paper.

Acknowledgments

This work was supported by FAPESP, CNPq, FAPDF (Grant No. 03/2025 – FAPDF PUBLICA), and by the University of Brasília through the DPI/BCE Grant No. 001/2025. The authors would like to thank Prof. Cristiano Luis Pinto de Oliveira and Dr. Pedro Leonidas Oseliero Filho for the SAXS measurements, and Prof. Amando Ito (*in memoriam*) for the use of the time-resolved fluorimeter for the preliminary experiments.

Appendix A. Supplementary data

Supplementary data to this article can be found online at https://doi.org/10.1016/j.bbrep.2025.102128.

References

[1] N. Sayed, P. Allawadhi, A. Khurana, V. Singh, U. Navik, S.K. Pasumarthi, I. Khurana, A.K. Banothu, R. Weiskirchen, K.K. Bharani, Gene therapy: comprehensive overview and therapeutic applications, Life Sci. 294 (2022) 120375, https://doi.org/10.1016/j.lfs.2022.120375.

[2] A. Poddar, R. Banerjee, R. Shukla, Editorial: non-viral vectors for gene therapy/nucleic acid delivery, Front. Bioeng. Biotechnol. 11 (2023) 1304769, https://doi.org/10.3389/fbioe.2023.1304769.

[3] H. Zu, D. Gao, Non-viral vectors in gene therapy: recent development, challenges, and prospects, AAPS J. 23 (2021) 78, https://doi.org/10.1208/s12248-021-00608-7.

[4] C. Janich, C. Wölk, F. Erdmann, T. Groth, G. Brezesinski, B. Dobner, A. Langner, Composites of malonic acid diamides and phospholipids — impact of lipoplex stability on transfection efficiency, J. Contr. Release 220 (2015) 295–307, https://doi.org/10.1016/j.jconrel.2015.10.045.

[5] B. Ugarte-Uribe, S. Grijalvo, S.N. Pertíñez, J.V. Busto, C. Martín, A. Alagia, F. M. Goñi, R. Eritja, I. Alkorta, Lipid-modified oligonucleotide conjugates: insights into gene silencing, interaction with model membranes and cellular uptake mechanisms, Bioorg. Med. Chem. 25 (2017) 175–186, https://doi.org/10.1016/j.bmc.2016.10.024.

[6] J. Das, J.W. Han, Y.-J. Choi, H. Song, S.-G. Cho, C. Park, H.G. Seo, J.-H. Kim, Cationic lipid-nanoceria hybrids, a novel nonviral vector-mediated gene delivery into mammalian cells: investigation of the cellular uptake mechanism, Sci. Rep. 6 (2016) 29197, https://doi.org/10.1038/srep29197.

[7] J.H.K. Rozenfeld, S.R. Silva, P.A. Ranéia, E. Faquim-Mauro, A.M. Carmona-Ribeiro, Stable assemblies of cationic bilayer fragments and CpG oligonucleotide with enhanced immunoadjuvant activity in vivo, J. Contr. Release 160 (2012) 367–373, https://doi.org/10.1016/j.jconrel.2011.10.017.

[8] A.C.N. Oliveira, T.F. Martens, K. Raemdonck, R.D. Adati, E. Feitosa, C. Botelho, A. C. Gomes, K. Braeckmans, M.E.C.D. Real Oliveira, Dioctadecyldimethylammonium: Monoolein nanocarriers for efficient *in vitro* gene silencing, ACS Appl. Mater. Interfaces 6 (2014) 6977–6989, https://doi.org/10.1021/am500793y.

[9] J. Davidsen, I. Rosenkrands, D. Christensen, A. Vangala, D. Kirby, Y. Perrie, E. M. Agger, P. Andersen, Characterization of cationic liposomes based on dimethyldioctadecylammonium and synthetic cord factor from M. tuberculosis (trehalose 6,6′-dibehenate)—A novel adjuvant inducing both strong CMI and antibody responses, Biochim. Biophys. Acta BBA - Biomembr. 1718 (2005) 22–31, https://doi.org/10.1016/j.bbamem.2005.10.011.

[10] L.J. Carreño, S.S. Kharkwal, S.A. Porcelli, Optimizing NKT cell ligands as vaccine adjuvants, Immunotherapy 6 (2014) 309–320, https://doi.org/10.2217/imt.13.175.
[11] T.R. Oliveira, C.R. Benatti, M.T. Lamy, Structural characterization of the interaction of the polyene antibiotic amphotericin B with DODAB bicelles and vesicles, Biochim. Biophys. Acta BBA - Biomembr. 1808 (2011) 2629–2637, https://doi.org/10.1016/j.bbamem.2011.07.042.
[12] D.B. Vieira, L.F. Pacheco, A.M. Carmona-Ribeiro, Assembly of a model hydrophobic drug into cationic bilayer fragments, J. Colloid Interface Sci. 293 (2006) 240–247, https://doi.org/10.1016/j.jcis.2005.06.046.
[13] C. Carneiro, A. Correia, T. Collins, M. Vilanova, C. Pais, A.C. Gomes, M.E.C.D. Real Oliveira, P. Sampaio, DODAB:monoolein liposomes containing Candida albicans cell wall surface proteins: a novel adjuvant and delivery system, Eur. J. Pharm. Biopharm. 89 (2015) 190–200, https://doi.org/10.1016/j.ejpb.2014.11.028.
[14] T.C.S. Ferreira, I.P. Sauter, L. Borda-Samper, E. Bentivoglio, J.P. DaMata, N. N. Taniwaki, P.R. Orrego, J.E. Araya, N. Lincopan, M. Cortez, Effect of DODAB nano-sized cationic bilayer fragments against Leishmania amazonensis, Molecules 25 (2020) 5741, https://doi.org/10.3390/molecules25235741.
[15] L.S. Martins, D.A. Nomura, E.L. Duarte, K.A. Riske, M.T. Lamy, J.H.K. Rozenfeld, Structural characterization of cationic DODAB bilayers containing C24:1 β-glucosylceramide, Biochim. Biophys. Acta BBA - Biomembr. 1861 (2019) 643–650, https://doi.org/10.1016/j.bbamem.2018.12.018.
[16] L.S. Martins, E.L. Duarte, M.T. Lamy, J.H.K. Rozenfeld, Supramolecular organization of α-galactosylceramide in pure dispersions and in cationic DODAB bilayers, Chem. Phys. Lipids 232 (2020) 104963, https://doi.org/10.1016/j.chemphyslip.2020.104963.
[17] L.S. Martins, E.L. Duarte, M.T. Lamy, J.H.K. Rozenfeld, DODAB vesicles containing lysophosphatidylcholines: the relevance of acyl chain saturation on the membrane structure and thermal properties, Biophys. Chem. 300 (2023) 107075, https://doi.org/10.1016/j.bpc.2023.107075.
[18] L.R.M.M. Aps, M.B. Tavares, J.H.K. Rozenfeld, M.T. Lamy, L.C.S. Ferreira, M. O. Diniz, Bacterial spores as particulate carriers for gene gun delivery of plasmid DNA, J. Biotechnol. 228 (2016) 58–66, https://doi.org/10.1016/j.jbiotec.2016.04.027.
[19] A. Carmona-Ribeiro, Biomimetic nanoparticles: preparation, characterization and biomedical applications, Int. J. Nanomed. (2010) 249, https://doi.org/10.2147/IJN.S9035.
[20] S. Tassler, B. Dobner, L. Lampp, R. Ziółkowski, E. Malinowska, C. Wölk, G. Brezesinski, DNA delivery systems based on peptide-mimicking cationic lipids—the effect of the Co-Lipid on the structure and DNA binding capacity, Langmuir 35 (2019) 4613–4625, https://doi.org/10.1021/acs.langmuir.8b04139.
[21] C.I. Ochoa-Sánchez, K. Ochoa Lara, J.M. Martínez-Soto, A. Martínez-Higuera, R. A. Iñiguez-Palomares, R. Moreno-Corral, E. Rodríguez-León, A. Soto-Guzmán, C. Rodríguez-Beas, Physicochemical characterization and viability assays of a promising formulation of liposomes (DODAB-DOPC) in complexation with ctDNA, J. Nanomater. 2022 (2022) 1–10, https://doi.org/10.1155/2022/3085103.
[22] J.H.K. Rozenfeld, E.L. Duarte, L.R.S. Barbosa, M.T. Lamy, The effect of an oligonucleotide on the structure of cationic DODAB vesicles, Phys. Chem. Chem. Phys. 17 (2015) 7498–7506, https://doi.org/10.1039/C4CP05652C.
[23] M.K. Masukawa, C.C. Vequi-Suplicy, E.L. Duarte, M.T. Lamy, A closer look into laurdan as a probe to monitor cationic DODAB bilayers, J. Photochem. Photobiol. Chem. 376 (2019) 238–246, https://doi.org/10.1016/j.jphotochem.2019.03.006.
[24] P.C. Hiemenz, R. Rajagopalan, in: Principles of Colloid and Surface Chemistry 3, CRC, Taylor & Francis, Boca Raton, Fla, 1997 ev.expanded.
[25] G.S. Vignoli Muniz, E.L. Duarte, E.N. Lorenzón, E.M. Cilli, M.T. Lamy, What different physical techniques can disclose about disruptions on membrane structure caused by the antimicrobial peptide hylin a1 and a more positively charged analogue, Chem. Phys. Lipids 243 (2022) 105173, https://doi.org/10.1016/j.chemphyslip.2022.105173.
[26] A. Mendonça, A.C. Rocha, A.C. Duarte, E.B.H. Santos, The inner filter effects and their correction in fluorescence spectra of salt marsh humic matter, Anal. Chim. Acta 788 (2013) 99–107, https://doi.org/10.1016/j.aca.2013.05.051.
[27] E. Joseph, G. Singhvi, Multifunctional nanocrystals for cancer therapy: a potential nanocarrier, in: Nanomater. Drug Deliv. Ther., Elsevier, 2019, pp. 91–116, https://doi.org/10.1016/B978-0-12-816505-8.00007-2.
[28] S.R. Aragón, R. Pecora, Theory of dynamic light scattering from polydisperse systems, J. Chem. Phys. 64 (1976) 2395–2404, https://doi.org/10.1063/1.432528.
[29] J.H.K. Rozenfeld, T.R. Oliveira, M.T. Lamy, A.M. Carmona-Ribeiro, Interaction of cationic bilayer fragments with a model oligonucleotide, Biochim. Biophys. Acta BBA - Biomembr 1808 (2011) 649–655, https://doi.org/10.1016/j.bbamem.2010.11.036.
[30] B.D. Cullity, S.R. Stock, Elements of X-ray Diffraction, 3. ed, Prentice Hall, Upper Saddle River, NJ, 2001.
[31] A. Mishra, K.P. Tai, N.W. Schmidt, A.J. Ouellette, G.C.L. Wong, Small-angle X-ray scattering studies of peptide–lipid interactions using the mouse paneth cell α-Defensin Cryptdin-4, in: Methods Enzymol., Elsevier, 2011, pp. 127–149, https://doi.org/10.1016/B978-0-12-381268-1.00016-1.
[32] O. Glatter, O. Kratky (Eds.), Small Angle x-ray Scattering, Academic Press, London ; New York, 1982.
[33] G.A. Ferreira, W. Loh, Structural parameters of lamellar phases formed by the self-assembly of dialkyldimethylammonium bromides in aqueous solution, J. Braz. Chem. Soc. (2015), https://doi.org/10.5935/0103-5053.20150297.
[34] R.M. Fernandez, K.A. Riske, L.Q. Amaral, R. Itri, M.T. Lamy, Influence of salt on the structure of DMPG studied by SAXS and optical microscopy, Biochim. Biophys. Acta BBA - Biomembr. 1778 (2008) 907–916, https://doi.org/10.1016/j.bbamem.2007.12.005.
[35] F.M. Goñi, A. Alonso, Differential scanning calorimetry in the study of lipid structures, in: B. Larijani, ColinA. Rosser, R. Woscholski (Eds.), Chem. Biol., first ed., Wiley, 2006, pp. 47–66, https://doi.org/10.1002/9780470319253.ch4.
[36] J. Cocquyt, U. Olsson, G. Olofsson, P. Van Der Meeren, Thermal transitions of DODAB vesicular dispersions, Colloid Polym. Sci. 283 (2005) 1376–1381, https://doi.org/10.1007/s00396-005-1347-9.
[37] L. Coppola, M. Youssry, I. Nicotera, L. Gentile, Rheological investigation of thermal transitions in vesicular dispersion, J. Colloid Interface Sci. 338 (2009) 550–557, https://doi.org/10.1016/j.jcis.2009.06.054.
[38] P.S. Dubey, H. Srinivasan, V.K. Sharma, S. Mitra, V.G. Sakai, R. Mukhopadhyay, Dynamical transitions and diffusion mechanism in DODAB bilayer, Sci. Rep. 8 (2018) 1862, https://doi.org/10.1038/s41598-018-19899-6.
[39] G.S. Vignoli Muniz, M.C. Souza, E.L. Duarte, M.T. Lamy, Comparing the interaction of the antibiotic levofloxacin with zwitterionic and anionic membranes: calorimetry, fluorescence, and spin label studies, Biochim. Biophys. Acta BBA - Biomembr. 1863 (2021) 183622, https://doi.org/10.1016/j.bbamem.2021.183622.
[40] D. Zweytick, B. Japelj, E. Mileykovskaya, M. Zorko, W. Dowhan, S.E. Blondelle, S. Riedl, R. Jerala, K. Lohner, N-acylated peptides derived from human lactoferricin perturb organization of cardiolipin and phosphatidylethanolamine in cell membranes and induce defects in Escherichia coli cell division, PLoS One 9 (2014) e90228, https://doi.org/10.1371/journal.pone.0090228.
[41] L.A. Bagatolli, LAURDAN fluorescence properties in membranes: a journey from the fluorometer to the microscope, in: Y. Mély, G. Duportail (Eds.), Fluoresc. Methods Study Biol. Membr., Springer Berlin Heidelberg, Berlin, Heidelberg, 2012, pp. 3–35, https://doi.org/10.1007/4243_2012_42.
[42] T. Parasassi, E.K. Krasnowska, L. Bagatolli, E. Gratton, Laurdan and prodan as polarity-sensitive fluorescent membrane probes, J. Fluoresc. 8 (1998) 365–373, https://doi.org/10.1023/A:1020528716621.
[43] G. Gunther, L. Malacrida, D.M. Jameson, E. Gratton, S.A. Sánchez, LAURDAN since weber: the quest for visualizing membrane heterogeneity, Acc. Chem. Res. 54 (2021) 976–987, https://doi.org/10.1021/acs.accounts.0c00687.
[44] B. Valeur, Molecular Fluorescence: Principles and Applications, Wiley-VCH, Weinheim ; New York, 2002.
[45] G. Weber, F.J. Farris, Synthesis and spectral properties of a hydrophobic fluorescent probe: 6-propionyl-2-(dimethylamino)naphthalene, Biochemistry 18 (1979) 3075–3078, https://doi.org/10.1021/bi00581a025.
[46] C.C. De Vequi-Suplicy, C.R. Benatti, M.T. Lamy, Laurdan in fluid bilayers: position and structural sensitivity, J. Fluoresc. 16 (2006) 431–439, https://doi.org/10.1007/s10895-005-0059-3.
[47] C.C. Vequi-Suplicy, K. Coutinho, M.T. Lamy, New insights on the fluorescent emission spectra of prodan and laurdan, J. Fluoresc. 25 (2015) 621–629, https://doi.org/10.1007/s10895-015-1545-x.
[48] T. Parasassi, G. De Stasio, G. Ravagnan, R.M. Rusch, E. Gratton, Quantitation of lipid phases in phospholipid vesicles by the generalized polarization of laurdan fluorescence, Biophys. J. 60 (1991) 179–189, https://doi.org/10.1016/S0006-3495(91)82041-0.
[49] A.D. Lúcio, C.C. Vequi-Suplicy, R.M. Fernandez, M.T. Lamy, Laurdan spectrum decomposition as a tool for the analysis of surface bilayer structure and polarity: a study with DMPG, peptides and cholesterol, J. Fluoresc. 20 (2010) 473–482, https://doi.org/10.1007/s10895-009-0569-5.
[50] N.C. Santos, M. Prieto, M.A.R.B. Castanho, Quantifying molecular partition into model systems of biomembranes: an emphasis on optical spectroscopic methods, Biochim. Biophys. Acta BBA - Biomembr. 1612 (2003) 123–135, https://doi.org/10.1016/S0005-2736(03)00112-3.